Journal Pre-proof

Using CETSA assay and a mathematical model to reveal dual Bcl-2/Mcl-1 inhibition and on-target mechanism for ABT-199 and S1

Zongwei Guo , Ting Song , Zuguang Xue , Peng Liu ,
Minhang Zhang , Xiaodong Zhang , Zhichao Zhang

Please cite this article as: Zongwei Guo , Ting Song , Zuguang Xue , Peng Liu , Minhang Zhang , Xiaodong Zhang , Zhichao Zhang , Using CETSA assay and a mathematical model to reveal dual Bcl-2/Mcl-1 inhibition and on-target mechanism for ABT-199 and S1, *European Journal of Pharmaceutical Sciences* (2019), doi: https://doi.org/10.1016/j.ejps.2019.105105

Using CETSA assay and a mathematical model to reveal dual Bcl-2/Mcl-1 inhibition and on-target mechanism for ABT-199 and **S1**

Zongwei Guo[a, +], Ting Song[b, +, *], Zuguang Xue[c], Peng Liu[a], Minhang Zhang[a], Xiaodong Zhang[b], Zhichao Zhang[b, *]

[a] State Key Laboratory of Fine Chemicals, School of Life Science and Technology, Dalian University of Technology, Dalian, China.

[b] State Key Laboratory of Fine Chemicals, School of Chemistry, Dalian University of Technology, Dalian, China.

[c] Department of Hematology, Second Affiliated Hospital, Dalian Medical University, Dalian, China.

[*], To whom correspondence may be addressed.

Email: zczhang@dlut.edu.cn (Zhichao Zhang); songting@dlut.edu.cn (Ting Song).

[+], These authors contribute equally to this paper.

Abbreviations: CETSA, cellular thermal shift assay; Bcl-2, B-cell lymphoma-2; BH3, Bcl-2 homology 3; SPR, surface plasmon resonance; ITC, isothermal titration calorimetry; FP, fluorescence polarization; ODEs, ordinary differential equations; MOMP, mitochondrial outer membrane permeabilization

Key Words: CETSA, BH3 mimetics, Bcl-2 family proteins, mathematical modelling

1. Introduction

Members of the B-cell lymphoma-2 (Bcl-2) protein family are critical regulators of apoptosis and the life-or-death decision is mainly determined by the interactions between three fractions of the Bcl-2 family: namely the anti-apoptotic subfamily (e.g., Bcl-2 and Mcl-1) and two pro-apoptotic fractions, the BH3-only proteins (e.g., Bim and Puma) and the death effectors (Bax, Bak) (Moldoveanu et al., 2014; Sharpe et al., 2004; Hinds et al., 2005). 'BH3 mimetic' represents a new class of cancer drugs that induces apoptosis of cancer cells by targeting various anti-apoptotic Bcl-2-like proteins, which has gained great success (Delbridge et al., 2015; Billard et al., 2013). Clinical trials of venetoclax/ABT-199, a specific inhibitor of Bcl-2, have led to its approval for a refractory form of chronic lymphocytic leukemia (Deeks et al., 2016). It inspired the development of more BH3 mimetic drug leads.

Using a mathematical modelling approach combined with experimental fitting can help identify the underlying mechanism of drug efficacy in cells. A well-established model using ordinary differential equations (ODEs) and mathematical simulations via Bcl-2's multi-protein interaction interplay has been successfully used to understand the life-or-death decision (Zhao et al., 2015; Chen et al., 2007; Lindner et al., 2013). For example, Prehn et al. utilized ODE model simulation to accurately predict individual death response of cancer cells to 5-fluorouracil/oxaliplatin (Lindner et al., 2013). Using the ODE model to examine whether an on-target or off-target mechanism underlying the efficacy of BH3 mimetics would promote accelerated safety assessment of drug candidates.

The target binding affinity governs biological activities of BH3 mimetics, as well as critical parameter for modelling, but the affinities of various BH3 mimetics (e.g., ABT-737, A-1210477, AT-101, **S1**) for the Bcl-2-like proteins differ greatly among the different compounds as well as between different assays including isothermal titration calorimetry (ITC), surface plasmon resonance (SPR) and fluorescence polarization (FP) (Lu et al., 2016; Casara et al., 2018; Song et al., 2016; Milani et al., 2017; Konopleva et al., 2006; Kotschy et al., 2016; Zhang et al., 2011; Zhang et al., 2013; Song et al., 2015). In addition, these *in vitro* binding assays cannot directly measure target binding in cells; instead it is monitored indirectly by studying downstream cellular response, e.g., disruption of Bcl-2 protein complexes with pro-apoptotic members, Bax/Bak activation, and cytochrome c release. Consequently, several drugs (e.g., AT-101) have failed in advanced clinical trials and later been shown to cause toxicity as a result of off-target effects (Ko et al., 2007; Hu et al., 2011). Therefore, methods that could evaluate target engagement of BH3 mimetics in cells are urgently needed.

The cellular thermal shift assay (CETSA), a recently established method, enables assessment of drug target engagement directly in cells based on ligand-induced changes in protein thermal stability (Martinez et al., 2013; Jafari et al., 2014; Jensen et al., 2015; Martinez and Nordlund, 2016). It has gained success in applying CETSA across multiple drug target classes including protein kinases and Bcl-2 family proteins (Scheele et al., 2018; Bai et al., 2014). Whether CETSA could recapitulate the rank-order correlation between *in vitro* binding assays for different BH3 mimetics have not been evaluated.

ABT-199's binding selectivity and low-nM binding affinity to Bcl-2 is well characterized by *in vitro* binding assays (Souers et al., 2013). Preclinical studies on ABT-199 showed a wide range of LC_{50} values from the nanomolar to low micromolar range against a panel of leukemia cell lines

(Pan et al., 2014; Schwartz et al., 2016). ABT-199's cellular activity at the low micromolar range is inconsistent with its low-nM binding affinity to Bcl-2. A deep understanding of ABT-199's lethality against these leukemic subsets is expected to promote the development of a combination strategy to enhance ABT-199's efficacy.

Herein, we used CETSA assay to evaluate the target binding potency of various BH3 mimetics (ABT-737, ABT-199, A-1210477) to Bcl-2 and Mcl-1, and validated that the method could provide affinity rank-order and selectivity in agreement with *in vitro* binding assays. The CETSA experiments showed that AT-101 and **S1** bind Bcl-2-like protein in cells. By using a mathematical model combined with experimental fitting, we revealed that both Bcl-2 and Mcl-1 binding contribute to ABT-199's lethality in a subset of leukemic cell lines (THP-1, JURKAT and OCI-AML3). ABT-199's lower binding affinity to Mcl-1 led to efficacy in these Mcl-1-high cells at the micromolar range. In addition, the result of model fitting with experimental data differentiates **S1** and AT-101 into BH3 mimetics with on-target and off-target mechanism respectively.

2. Materials and Methods

2.1. Cell culture and chemicals

The human lung carcinoma cell lines H82, H1688, H209, H187, SHP77, and H1048 were purchased from American Type Culture Collection (Manassas, VA, USA). The human leukaemic cell lines RS4;11, HL-60, MOLM-13, THP-1, JURKAT, OCI-AML3 and the human breast carcinoma cell line MCF-7 were obtained from the Typical Culture Preservation Commission Cell Bank (Chinese Acadamy of Sciences, Shanghai, China). They were all used within 6 months from resuscitation. The 6 SCLC cell lines and 6 leukaemic cell lines were cultured at 37 °C in RMPI-1640 (Hyclone, Beijing, China) supplemented with 10% fetal bovine serum (Gibco Company, USA), 1% penicillin/streptomycin mixture (Hyclone, Beijing, China) in humidified atmosphere containing 5% CO_2. The growth medium for MCF-7 was DMEM-high glucose (Hyclone, Beijing, China). ABT-737, ABT-199, A-1210477 and AT-101 were purchased from Selleck Chemicals (Shanghai, China). **S1** was synthesized as previously described (Zhang et al., 2011) and dissolved in DMSO (10 mM) and was subsequently stored as stock solutions in dark-colored bottles at 4 °C before use.

2.2. Computational modelling

A previously well-established apoptotic network was used for modelling (Zhao et al., 2015; Chen et al., 2007; Lindner et al., 2013). The network focused on the regulation of mitochondrial outer membrane permeabilization (MOMP). Upon Bax and Bak activation by activator BH3-only proteins, they formed homo- or hetero-dimerization to induce MOMP. Bcl-2 family members can be classified into two groups: pro- and anti-apoptotic factors. The former contains the following two subtypes: the MOMP effectors Bax and Bak; the select BH3-only proteins termed "activators" (Bim and Puma). Anti-apoptotic Bcl-2 and Mcl-1 inhibit MOMP by binding these activators and effectors.

We used a set of ordinary differential equations (ODEs) to describe protein production,

degradation and interaction with mass-action kinetics (a detailed guideline was listed in Table S1-S6). ODEs were solved using MATLAB (The MathWorks Inc., Natick, MA, US) (RRID:SCR_001622) function *ode 15s*. The chemotherapeutic dose was used as model inputs. ABT-199, **S1** or AT-101 acted by binding to and inhibiting anti-apoptotic proteins with FP-based K_i values as target-drug interaction parameters. For details, see Table S5.

2.3. Cell apoptosis assay

Apoptosis was determined by the flow cytometric measurement of phosphatidylserine exposure using Annexin V-FITC. According to the manufacturer's instructions, cells were washed twice with phosphate buffered saline (PBS) and incubated with a 1:40 solution of FITC-conjugated Annexin V (Nanjing KeyGen BioTech Co., Ltd., Nanjing, China) in the dark for 10 min at room temperature. The Annexin V-FITC positive cells were analyzed by flow cytometry on a BD FACSCalibur (BD Biosciences). Cell Questc software (BD Biosciences) was used to determine the percentage of apoptosis in the samples. The Lethal Concentration 50 (LC_{50}) was defined as the concentration of small-molecule inhibitors to kill 50% of cells.

2.4. Immunoblotting

Whole-cell lysates were prepared by incubating cell pellets in RIPA buffer (Solarbio, Beijing, China) containing Halt protease inhibitor cocktail (Pierce Biotechnology, Rockford, USA) for 30 minutes on ice and centrifuged at 12,000 g for 15 minutes at 4 °C. Protein concentration of the supernatant was determined by BCA assay (Beyotime, Shanghai, China) and 100 μg of total protein was heated (95 °C, 10 minutes) in 5 × sample loading buffer (Sangon Biotech, Shanghai, China) and resolved in 15% SDS–PAGE. Proteins were then transferred to PVDF membranes using the Bio-Rad system, blocked for 60 minutes in phosphate buffered saline with 0.1% Tween (PBST) containing 5% skim milk (BD Biosciences, USA) and incubated with primary antibody overnight in PBST at 4 °C. Blots were washed with PBST and incubated with HRP-conjugated secondary antibody for 60 minutes at room temperature. Immune complexes were visualized by the use of Super Signal West Pico Chemiluminescent Substrate (Pierce Biotechnology) and detected on a Kodak Image Station 4000MM Pro (New Haven, CT, USA). Primary and Secondary antibodies used: Bcl-2 (#2870), Mcl-1 (#94296), Bcl-xL (#2762), Bim (#2933), Puma (#12450) were from CST (Cell Signaling Technologies, MA, USA). Bak (sc-517390), Bax (sc-7480), Actin (sc-8432) were from Santa Cruz (Santa Cruz Biotechnology, CA, USA). β-tubulin (#A01030) was from Abbkine (Abbkine Scientific Co., Ltd., Wuhan, China) and Cytochrome C (#AF2047) were from Beyotime. Anti-mouse IgG (H+L) (#A0216) and Anti-rabbit IgG (H+L) (#A0208) were from Beyotime.

2.5. Cytochrome c release assay

Mitochondrial fractions were isolated using Minute Mitochondrial Isolation kit for cells (Invent Biotechnologies, Beijing, China) according to the manufacturer's protocol. The isolated mitochondria fractions solubilizing in Non-denatured Protein Solubilization reagent (Invent Biotechnologies) and the supernatant (cytosolic fraction) were collected and subjected to

immunoblotting for Cytochrome c.

2.6. Co-immunoprecipitation

Harvested cells were lysed in 1% Triton buffer (Beyotime). Whole-cell lysates were obtained, 1 mg total proteins were precleared with protein A+G Agarose and incubated overnight with 1 μg of the specific antibody. Immunocomplexes were captured with protein A+G Agarose (Beyotime). The presence of immunocomplexes was determined by immunoblotting analysis.

2.7. Determination of intracellular protein concentration by quantitative immunoblotting

Cells were harvested, counted and lysed in RIPA buffer for 30 minutes on ice and centrifuged at 12,000 g for 15 minutes at 4 °C, supernatant was collected and intracellular protein concentration was determined by subsequent quantitative immunoblotting.

For quantitative immunoblotting, standard curves of each protein relating blot intensity to mass of loading were constructed with varying concentrations (0.1–10.0 ng) of 6 purified recombinant Bcl-2 family proteins and 20 μg of HL-60 extract. Recombinant human Bcl-2 and Mcl-1 were obtained as our report described (Zhang et al., 2011), Bim (LY416580), Puma (TP325345), Bax (RC204368), Bak (RC201216) were purchased from OriGene (Beijing, China). Immunoblotting images were acquired using a Kodak Image Station 4000MM Pro (New Haven, CT, USA) and densitometry was conducted using Kodak Carestream Molecular Imaging software. The total mass of the investigated proteins (Bcl-2, Mcl-1, Bim, Puma, BAX, BAK) in cell lysates from HL-60 was obtained from the calibration curves. Then, assuming a HL-60 cell volume of 1.11 pL (Schonbrun et al., 2013) and the appropriate molecular weights for Bcl-2, Mcl-1, Bim, Puma, BAX, BAK, cellular concentrations for these proteins were calculated. Protein concentrations in the other cell lines (H82, H1688, H209, H187, THP-1, SHP77, H1048, RS4;11, MOLM-13, THP-1, JURKAT, OCI-AML3) were determined by comparison to signals from HL-60 cell extracts.

Protein concentrations of Bcl-2, Mcl-1, Bim, Puma, BAX, BAK from cancer cell lines as determined by quantitative immunoblotting were used in calculations as initial and steady state concentrations in the model. Therefore, a panel of cell lines (H82, H1688, H209, H187, HL-60, THP-1, SHP77 and H1048) were used to study **S1**, AT-101 and another panel of cell lines (RS4;11, HL-60, MOLM-13, THP-1, JURKAT, OCI-AML3) were used to study ABT-199.

2.8. Cellular Thermal Shift Assay (CETSA)

For the CETSA assay, cultured cells (approximately 30 million cells are required to establish one melting curve) were harvested and resuspended with culture medium to a cell density of 5 million cells per ml and seeded into T25 flasks (Coring Plastics). Cells were treated with either ABT-199, A-1210477 or vehicle (DMSO) for 1 h in an incubator at 37 °C and 5% CO2. The cell suspensions were collected and diluted with PBS, then divided into 100 μL aliquots in PCR 0.2 ml tubes and heated at designated temperatures (40-64 °C for Bcl-2, 42-66 °C for Mcl-1) for 3 min in a PCR machine (ProFlex, Applied Biosystems) followed by 3 min of cooling at room temperature. The heat-treated cell suspensions were freeze-thawed twice using liquid nitrogen and a heating

block set at 25 °C. The resulting cell lysates were centrifuged at 20,000 × g for 20 min at 4 °C. The supernatant was transferred to new microtube from the cell debris and aggregates, and then analyzed by Western blot. ABT-199 and A-1210477 were added from DMSO stocks to the final concentration of 100 μM and DMSO concentration 1%. Control samples were incubated with an equal amount of DMSO.

For the ITDRF$_{CETSA}$ assay, cultured cells were harvested and treated with ABT-199, ABT-737, A-1210477, AT-101, **S1**, respectively. The five inhibitors were serially diluted to generate a six points dose–response curve with ten-fold difference in concentration between each point. Cells were treated with each respective compound concentrations and one vehicle (DMSO) as control in 100 μL aliquots in PCR 0.2 ml tubes for 1 h in an incubator at 37 °C and 5% CO2. The cell aliquots were heated at 60 °C for Bcl-2 and 62 °C for Mcl-1 respectively following the procedure described above. The heat-treated cell suspensions were freeze-thawed and centrifuged to discard the precipitates, then the remaining soluble fraction was analyzed with Western blot.

β-actin or β-tubulin levels were used to normalize the intensities of target proteins. For the CETSA curves the relative band intensities were related to the intensities of the lowest temperature for the drug exposed samples and control samples, respectively. For the ITDRF$_{CETSA}$ curves the relative band intensities were related to control samples.

2.9. Statistical analysis

Statistical significance was determined with mean ± standard deviation(sd) by two-tailed t-test using SPSS 18.0 software (SPSS, Inc., Chicago, MI, USA). P values in between $0.01 < P < 0.05$ were considered significant (*) and very significant (**) when $0.001 < P < 0.01$.

A correlation analysis was performed to determine the relationship between the LC$_{50}$ values of cell apoptosis and the model predicted dose ω that is required to induce MOMP. The grade of liner dependency was assessed by Pearson's correlation coefficient. For analysis, the MATLAB function *corr* was used. A correlation coefficient being close to or equal to one was assumed to indicate a good correlation.

3. Results

3.1. Validating target engagement of BH3 mimetics in cells using the CETSA assays

The screen and optimization of BH3 mimetics often rely on *in vitro* biochemical assays (FP, SPR or ITC) using recombinant Bcl-2-like proteins (Bcl-2, Mcl-1). Whether the *in vitro* binding affinity could reflect target engagement in living cells is ambiguous and needs to be answered for validating authentic BH3 mimetics, whose therapeutic effect should be achieved through direct binding of Bcl-2-like proteins. CETSA is a recently established method for monitoring target engagement in cells. To evaluate the binding potency of BH3 mimetics to Bcl-2 proteins in living cells, we applied a CETSA assay on a series of BH3 mimetics (ABT-199, ABT-737, A-1210477, AT-101 and **S1**) which have different binding profile, and compared the half-saturation points (IC$_{50}$) determined using isothermal dose-response fingerprinting (ITDRF$_{CETSA}$) with their reported *in vitro* binding affinities.

Firstly, the temperature for the ITDRF$_{CETSA}$ experiment was determined by detecting the

thermal melt curves of Bcl-2 and Mcl-1 in untreated cells or under the saturated binding with BH3 mimetics. T_m, which is the temperature where half of the protein is denatured was calculated for $ITDRF_{CETSA}$ experiment. As shown by the thermal melt curves, in the absence of BH3 mimetics, Bcl-2 and Mcl-1 proteins lost their higher-order structure and denature at 60 °C and 62 °C respectively (Fig. 1A and B). In the presence of ABT-199 or A-1210477 (adding 100 μM for saturated binding), the stabilities of Bcl-2 and Mcl-1 proteins, but not of the control protein β-actin, were significantly enhanced. When the heating temperature was further raised to 64 °C and 66 °C respectively for Bcl-2 and Mcl-1, they cannot be stabilized by ABT-199 or A-1210477 (Fig. 1A and B). A significant T_m shift, which is dependent on the intrinsic affinity of the ligand was observed at saturating inhibitor concentrations (Bcl-2 for 4.3 °C and Mcl-1 for 3.9 °C).

In addition to Bcl-2 and Mcl-1 proteins, we assayed the melt curves of BH3-only proteins and observed that the melting temperatures were much lower than that of Bcl-2 and Mcl-1($T_m = 57.2 \pm 0.28$ °C and 59.2 ± 0.21 °C respectively), as exemplified by Bim and Puma ($T_m = 45.2 \pm 0.23$ °C and 44.8 ± 0.25 °C respectively) (Supplementary Fig. 1). It is consistent with the intrinsically disordered property of BH3-only proteins (Wiggins et al., 2011; Rogers et al., 2014). The following $ITDRF_{CETSA}$ experiment assay was performed at >=60 °C, under which Bim and Puma should be completely denatured. The effect of small-molecule binding on thermal stabilities of Bcl-2 and Mcl-1 cannot be influenced by Puma and Bim.

Then, we performed $ITDRF_{CETSA}$ experiments with cells after treatment with a concentration gradient of ABT-199, ABT-737 or A-1210477 ranging from 1 nM to 100 μM. The dose-response curve derived from densitometry of the immunoblotting was portrayed in Fig. 1C and D, right panel, from which the IC_{50} was obtained and compared to reported competitive inhibitor constant (K_i) and dissociation constant (K_d) values. As shown in Table 1, the CETSA-based experiments detected the IC_{50} values of 3.6 and 40 nM respectively for ABT-199 and ABT-737 binding Bcl-2, and IC_{50} values of 0.8 nM for A-1210477 binding Mcl-1, which were consistent with their *in vitro* binding affinity rank-order (Lu et al., 2016; Casara et al., 2018; Song et al., 2016; Milani et al., 2017; Konopleva et al., 2006; Kotschy et al., 2016; Zhang et al., 2011; Zhang et al., 2013; Song et al., 2015). In addition, the binding selectivity profile of ABT-199, ABT-737 and A-1210477 could be recapitulated by CETSA-based IC_{50} values (Table 1). The results suggested that $ITDRF_{CETSA}$ could provide evidence on determining whether the *in vitro* binding assay could resemble that in living cells. In addition, as shown by the $ITDRF_{CETSA}$ curve for Mcl-1 proteins, ABT-199 and ABT-737 can also bind and stabilize Mcl-1 in a dose-dependent manner with an IC_{50} value of 1 and 8.3 μM, respectively. It strongly suggested that ABT compounds could target Mcl-1 in cells at the micromolar range, which is much higher than their effective concentrations on Bcl-2.

S1 and AT-101 were developed as pan-BH3 mimetics that bind Bcl-2 and Mcl-1 with comparable affinities, but they were argued to induce apoptosis in cells through direct targeting Bcl-2 and Mcl-1. For example, Eastman and co-workers reported that **S1** does not function as a pan-Bcl-2 inhibitor in cells but rather it upregulates the BH3-only protein Noxa, which inhibits Mcl-1 and then leads to apoptosis (Albershardt et al., 2011). To monitor the target engagement of **S1** and AT-101 in cells, we performed $ITDRF_{CETSA}$ experiments with cells after treatment with a concentration gradient of **S1** and AT-101. As shown in Fig. 1C and D, both of them could stabilize cellular Bcl-2 and Mcl-1 proteins with a dose-response manner at the sub-micromolar range, confirming target engagement in living cells. The CETSA-based IC_{50} values of **S1** showed relatively higher binding affinities to Mcl-1 and Bcl-2 (120 and 210 nM, respectively) than that of

7

AT-101 (208 and 420 nM, respectively) (Table 1), which was consistent with the rank-order of their competitive binding abilities determined by FP (Table 1). The CETSA assay provided evidence supporting that **S1** and AT-101 could directly hit Bcl-2 and Mcl-1 in living cells.

3.2. Modelling of MOMP predicted an on-target cell death induced by S1, rather than AT-101

To further explore whether **S1** or AT-101 act in cells totally through an on-target mechanism, which is marked by that target occupancy could be translated to pharmacological response in a different cellular context, we utilized a modeling method (Fig. 2A, for details, see supplementary materials). Due to the pro-survival role in platelets, Bcl-xL has an on-target toxicity effect (Mason et al., 2007; Zhang et al., 2007). For practical use, cancer cells expressing low Bcl-xL level are treatment target. Therefore, we selected cancer cell lines that express certain amounts of Bcl-2 and Mcl-1, but few Bcl-xL as experimental and model examples. A panel of leukemia and lung cancer cell lines (H82, H1688, H209, H187, HL-60, THP-1, SHP77 and H1048) that express relatively low levels of Bcl-xL were modelled to calculate the doses of BH3 mimetics (dose η) required to induce MOMP. The FP-based binding affinities of **S1** and AT-101 were parameterized for target protein-inhibitor interaction (Supplementary Table S1). Different doses of BH3 mimetics were used as input, whose level combined with binding affinity determined the extent of target occupancy and that led to dissociation of pro- and anti-apoptotic proteins resulting in effector (Bax and Bak) oligomerization. MOMP was assumed to occur when more than 10% of total effectors for oligomers (Lindner et al., 2013). The levels of anti-apoptotic proteins Bcl-2, Mcl-1, Bax, Bak, Bim, Puma were quantified (Fig. 2B and Supplementary Fig. 2) and modeled to attenuate MOMP by engaging the activator BH3-only protein (Bim and Puma) and effectors (Supplementary Table S1-S6). Since the levels of Bcl-xL in our selected cell lines were very low, we assumed that the specie in model did not participate in reactions.

A wide range of dose η was calculated for **S1** or AT-101 to induce MOMP in different cell lines. To investigate whether model predictions correlate to the pharmacological response, we compared calculated dose η with experimentally determined LC_{50} (Supplementary Fig. 3). Results of our analysis are depicted in Fig. 2C and D. For **S1**, the calculated dose η showed a positive correlation with experimental LC_{50} ($r = 0.83$, $P = 0.01$), suggesting that Bcl-2 and Mcl-1's binding accounts for **S1**'s pharmacological response. In contrast, no significant correlation was observed for AT-101 between calculated dose η with experimental LC_{50} ($r = 0.02$, $P = 0.15$), suggesting that an off-target mechanism is involved in antitumor efficacy of AT-101, which is consistent with previous reports (Ko et al., 2007; Hu et al., 2011).

3.3. Modelling combined with cellular experiments revealed that dual engagement of Bcl-2 and Mcl-1 underlies ABT-199's pharmacological response in leukemic subsets

The observation on direct targeting cellular Mcl-1 by ABT-199 with a half-saturation binding potency at 1 μM argued that ABT-199's lethality is Bcl-2 target-dependent. To explore if Mcl-1 also contribute to ABT-199's lethality, we evaluated the pharmacological response of ABT-199 in a panel of leukemic cell lines (RS4;11, HL-60, MOLM-13, THP-1, JURKAT and OCI-AML3) which expressed certain levels of Bcl-2, Mcl-1 and few Bcl-xL protein. Cell apoptosis assay was

performed and a wide range of LC_{50} was obtained for the 6 cell lines (Fig. 3A). Compared with RS4;11, HL-60 and MOLM-13 cells that exhibited lower LC_{50} in response to ABT-199 (0.06, 0.12 and 0.32 μM), significantly greater amounts of Mcl-1 were detected in THP-1, JURKAT and OCI-AML3 cells that exhibited higher LC_{50} values (1.3, 4.5 and 7.8 μM).

The absolute amounts of Bcl-2 and Mcl-1 proteins were quantified in these leukemic cell lines (Fig. 3A and Supplementary Fig. 2) and modeled to antagonize MOMP. FP-based K_i values were parameterized for characterizing ABT-199's interaction with Bcl-2 and Mcl-1 (Model I). Previous FP-based binding assays showed that ABT-199 binds Mcl-1 with a K_i value above 0.78 μM, and we used the value to approximate the binding process in Model I. For comparison, we constructed Model II assuming that ABT-199 cannot bind Mcl-1 at all. Then, we calculated the dose η of ABT-199 required for MOMP by using Model I and Model II, respectively, and compared them with experimental LC_{50} values. As shown in Fig. 3B and C, Model I showed a positive correlation with experimental LC_{50} values ($r = 0.87$, $P = 0.01$), but Model II did not show correlation ($r = 0.11$, $P = 0.13$). Indeed, for RS4;11, HL-60 and MOLM-13 cells that express low levels of Mcl-1, an agreement between experimental LC_{50} with predicted dose η was gained by both model I and II (Fig. 3C, lower left corner). However, for THP-1, JURKAT and OCI-AML3 cells that express high levels of Mcl-1, experimental LC_{50} gained agreement with model I, but not with Model II, suggesting that Mcl-1 targeting contributes to ABT-199's lethality in the Mcl-1 high cell lines. To further evaluate the mechanism, we treated OCI-AML3 cells with a gradient dose of ABT-199, followed by immunoprecipitation of Mcl-1 and Bcl-2, respectively. Meanwhile, cytochrome c release was detected to monitor MOMP. As shown in Fig. 3D, 0.1 μM ABT-199 could displace nearly total Bim and Bax from Bcl-2 complexes, but nearly no cytochrome c release is detected. When the dose of ABT-199 is raised to 1 and 10 μM, displacement of Bim and Bak from Mcl-1 complexes is detected, which is accompanied with cytochrome c release. Taken together, modelling combined with experimental data demonstrated that ABT-199's lethality in leukemic subsets that express high levels of Mcl-1 is achieved by dual engagement of Bcl-2 and Mcl-1.

4. Discussion

We have made an evaluation of CETSA experiments for assessment of BH3 mimetics binding potency to Bcl-2-like proteins in cells. By using CETSA to rank the binding affinity order of control BH3 mimetics ABT-199, ABT-737 and A-1210477 toward Bcl-2 and Mcl-1, it is validated that the method could provide direct clues on evaluating binding affinity rank and selectivity on other BH3 mimetics. It fills in defect of *in vitro* binding affinities assayed (e.g., ITC, SPR or FP) (Lu et al., 2016; Casara et al., 2018; Song et al., 2016; Milani et al., 2017; Konopleva et al., 2006; Kotschy et al., 2016; Zhang et al., 2011; Zhang et al., 2013; Song et al., 2015).

In this study, by using CETSA experiments, another two BH3 mimetics **S1** and AT-101 were identified that directly bind Bcl-2 and Mcl-1 in cells, and the binding affinity order is consistent with previous *in vitro* binding assays. However, when integrating their binding affinities into a mathematical model that has been established to predict apoptosis responses to chemotherapy, only **S1**, but not AT-101, gained agreement with experimental LC_{50}. For **S1**, it existed opposite opinions on its mechanism of action. One report showed that **S1** acted indirectly through BH3-only proteins (Albershardt et al., 2011). In another study, **S1** was shown that kill cancer cells in a Bax/Bak-dependent manner (Zhang et al., 2011), which is a hallmark of authentic BH3

mimetic. Herein, combined the CETSA experiments and modelling study results, an on-target mechanism of **S1** was supported. As for AT-101, an inconsistency between modelling and experiments indicates an off-target mechanism, which is also consistent with previous reports (Ko et al., 2007; Hu et al., 2011).

Recently, AT101 has also been reported with multiple targets, e.g., YAP/TAZ, EGFRL858R/T790M, α-reductase 1, 3α-hydroxysteroid dehydrogenase, retinol dehydrogenase 2, CHEK1 and CHEK2 (Xu et al., 2019; Linder et al., 2019; Cao et al., 2019;). Compared with ABT-199, AT-101 presents a complex three-dimensional structure, AT-101 is composed of two smaller planar aromatic structures substituted with multi-hydroxyl groups. The smaller planar structure is more adaptable to the extensively existed small "grooves" on the surface of different kinds of proteins, and the multi-hydroxyl groups can form H-bonds with backbone amide groups and side chain hydrophilic groups of residues on protein surfaces. All these reasons suggest that AT-101 has the potential to bind in the small "grooves" on the surface of different kinds of proteins, leading to a multi-target binding property. In comparison, ABT-199 with complex three-dimensional structure will suffer from steric hindrance when binding to these small "grooves", and thus can only adapt to the large, flat protein-protein interaction groove in Bcl-2.

Venetoclax (ABT-199) has received FDA approval for the treatment of chronic lymphocytic leukemia (CLL) with 17p deletion (Deeks et al., 2016). By *in vitro* binding assay, ABT-199 was identified as a highly specific Bcl-2 inhibitor with nM affinity to Bcl-2 and nearly undetectable affinity to other Bcl-2-like proteins (Souers et al., 2013). In our CETSA assay, we detected that ABT-199 could bind and stabilize Mcl-1 upon heating, but the effect is much weaker than that for Bcl-2 ($IC_{50} = 1$ μM for Mcl-1 versus 3.6 nM for Bcl-2). Of note, our modelling study identified that the weak Mcl-1 binding in combination with Bcl-2 binding contributes to ABT-199's lethality in Mcl-1-high leukemia cell lines (THP-1, JURKAT and OCI-AML3). It resulted in ABT-199's dose required to induce apoptosis are in the micromolar range, as shown by model predicted dose η and cell-based assay. Given on that the peak plasma concentration is at least 3-fold higher than the LC_{50} values in cell-based experiments (Schuler et al., 2002), therapeutically reachable concentration cannot be gained for ABT-199 in clinical treatment. It implied that agents that are effective at suppressing Mcl-1 need to be combined with ABT-199 to treat patients with cancer cells expressing high levels of Mcl-1.

Declaration of interest

Acknowledgements

References

Albershardt T.C., Salerni B.L., Soderquist R.S., Bates D.J., Pletnev A.A., Kisselev A.F., Eastman A., 2011. Multiple BH3 mimetics antagonize antiapoptotic MCL1 protein by inducing the endoplasmic reticulum stress response and up-regulating BH3-only protein Noxa. J. Biol. Chem. 286, 24882-24895.

Bai L., Chen J., McEachern D., Liu L., Zhou H., Aguilar A., Wang S., 2014. BM-1197: A Novel and Specific Bcl-2/Bcl-xL Inhibitor Inducing Complete and Long-Lasting Tumor Regression In Vivo. Plos One 9, e99404.

Billard C., 2013. BH3 mimetics: status of the field and new developments. Mol. Cancer Ther. 12, 1691-1700.

Cao, S., Wang, G., Ge, F., Li, X., Zhu, Q., Ge, R. S., & Wang, Y., 2019. Gossypol inhibits 5α-reductase 1 and 3α-hydroxysteroid dehydrogenase: Its possible use for the treatment of prostate cancer. Fitoterapia 133, 102-108.

Casara P., Davidson J., Claperon A., et al., 2018. S55746 is a novel orally active BCL-2 selective and potent inhibitor that impairs hematological tumor growth. Oncotarget 9, 20075.

Chen C., Cui J., Zhang W., Shen P., 2007. Robustness analysis identifies the plausible model of the Bcl-2 apoptotic switch. FEBS Lett. 581, 5143-5150.

Deeks, E.D., 2016. Venetoclax: first global approval. Drugs 76, 979-987.

Delbridge A.R.D., Strasser A., 2015. The BCL-2 protein family, BH3-mimetics and cancer therapy. Cell Death Differ. 22, 1071-1080.

Hinds M.G., Day C.L., 2005. Regulation of apoptosis: Uncovering the binding determinants. Curr. Opin. Struct. Biol. 15, 690–699.

Hu Z.Y., Wang J., Cheng G., Zhu X.F., Huang P., Yang D., Zeng Y.X., 2011. Apogossypolone targets mitochondria and light enhances its anticancer activity by stimulating generation of singlet oxygen and reactive oxygen species. Chin. J. Cancer 30, 41-53.

Jafari, R., Almqvist, H., Axelsson, H., Ignatushchenko, M., Lundbäck, T., Nordlund, P., & Molina, D.M., 2014. The cellular thermal shift assay for evaluating drug target interactions in cells. Nat. Protoc. 9, 2100.

Jensen A.J., Molina D.M., Lundbäck T., 2015. CETSA: a target engagement assay with potential to transform drug discovery. Future Med. Chem. 7, 975-978.

Linder, B., Wehle, A., Hehlgans, S., Bonn, F., Dikic, I., Rödel, F., & Kögel,D., 2019. Arsenic Trioxide and (−)-Gossypol Synergistically Target Glioma Stem-Like Cells via Inhibition of Hedgehog and Notch Signaling. Cancers 11, 350.

Lindner A.U., Concannon C.G., Boukes G.J., Cannon M.D., Liambi F., Ryan D., et al., 2013. Systems analysis of Bcl-2 protein family interactions establishes a model to predict responses to chemotherapy. Cancer Res. 73, 519-528.

Lu Y., Wu S., Yue Y., et al., 2016. Gossypol with hydrophobic linear esters exhibits enhanced

antitumor activity as an inhibitor of antiapoptotic proteins. ACS Med. Chem. Lett. 7, 1185-1190.

Ko C.H., Shen S.C., Yang L.Y., Lin C.W., Chen Y.C., 2007. Gossypol reduction of tumor growth through ROS-dependent mitochondria pathway in human colorectal carcinoma cells. Int. J. Cancer 121, 1670-1679.

Konopleva, M., Contractor, R., Tsao, T., Samudio, I., Ruvolo, P.P., Kitada, S., Verhaegen, M., 2006. Mechanisms of apoptosis sensitivity and resistance to the BH3 mimetic ABT-737 in acute myeloid leukemia. Cancer Cell 10, 375-388.

Kotschy, A., Szlavik, Z., Murray, J., Davidson, J., Maragno, A.L., Le Toumelin-Braizat, G., Bruno, A., 2016. The MCL1 inhibitor S63845 is tolerable and effective in diverse cancer models. Nature 538, 477.

Martinez D.M., Jafari R., Ignatushchenko M., Seki T., Larsson E.A., Dan C., Sreekumar L., Cao Y., Nordlund P., 2013. Monitoring drug target engagement in cells and tissues using the cellular thermal shift assay. Science 341, 84-87.

Martinez D.M., Nordlund P., 2016. The cellular thermal shift assay: a novel biophysical assay for in situ drug target engagement and mechanistic biomarker studies. Annu. Rev. Pharmacol. Toxicol. 56, 141-161.

Milani, M., Byrne, D.P., Greaves, G., Butterworth, M., Cohen, G.M., Eyers, P. A., Varadarajan, S., 2017. DRP-1 is required for BH3 mimetic-mediated mitochondrial fragmentation and apoptosis. Cell Death Dis. 8, e2552.

Moldoveanu, T., Follis, A.V., Kriwacki, R.W., & Green, D.R., 2014. Many players in BCL-2 family affairs. Trends Biochem. Sci. 39, 101-111.

Pan R., Hogdal L.J., Benito J.M., Bucci D., Han L., Borthakur G., Cortes J., DeAngelo D.J., Debose L., Mu H., et al., 2014. Selective BCL-2 Inhibition by ABT-199 Causes On Target Cell Death in Acute Myeloid Leukemia. Cancer Discov. 4, 362-375.

Park, D., Magis, A.T., Li, R., Owonikoko, T.K., Sica, G.L., Sun, S.Y., & Deng, X. 2013. Novel small-molecule inhibitors of Bcl-XL to treat lung cancer. Cancer Res. 73, 5485-5496.

Rogers J.M., Wong C.T., Clarke J., 2014. Coupled Folding and Binding of the Disordered Protein PUMA Does Not Require Particular Residue Structure. J. Am. Chem. Soc. 136, 5197-5200.

Scheele S., Geiger J.A., DeRocher A.E., Choi R., Smith T.R., Hulverson M.A., Vidadala R.S.R., Barrett L.K., Maly D.J., Merritt E.A., Ojo K.K., Van Voorhis W.C., Parsons M., 2018. Toxoplasma Calcium-Dependent Protein Kinase 1 Inhibitors: Probing Activity and Resistance Using Cellular Thermal Shift Assays. Antimicrob. Agents Chemother. 62, e00051-18.

Schuler P.J., Trellakis S., Greve J., Bas M., Bergmann C., Bolke E., et al., 2002. In vitro chemosensitivity of head and neck cancer cell lines. Eur. J. Med. Res. 15, 337-344.

Schwartz J., Niu X., Walton E., Hurley L., Lin H., Edwards H., Taub J.W., Wang Z., Ge Y., 2016. Synergistic anti-leukemic interactions between ABT-199 and panobinostat in acute myeloid leukemia ex vivo. Am. J. Transl. Res. 8, 3893-3902.

Sharpe, J.C., Arnoult, D., Youle, R.J., 2004. Control of mitochondrial permeability by Bcl-2 family members. Biochim. Biophys. Acta 1644, 107-113.

Song, T., Yu, X., Liu, Y., Li, X., Chai, G., Zhang, Z., 2015. Discovery of a Small-Molecule pBcl-2 Inhibitor that Overcomes pBcl-2-Mediated Resistance to Apoptosis. ChemBioChem 16, 757-765.

Song, T., Chai, G., Liu, Y., Yu, X., Wang, Z., Zhang, Z., 2016. Bcl-2 phosphorylation confers resistance on chronic lymphocytic leukaemia cells to the BH3 mimetics ABT-737, ABT-263 and ABT-199 by impeding direct binding. Brit. J. Pharmacol. 173, 471-483.

Souers A.J., Leverson J.D., Boghaert E.R., et al., 2013. ABT-199, a potent and selective Bcl-2 inhibitor achieves antitumor activity while sparing platelets. Nat. Med. 19, 202-208.

Wang, G., Nikolovska-Coleska, Z., Yang, C.Y., Wang, R., Tang, G., Guo, J., & Meagher, J., 2006. Structure-based design of potent small-molecule inhibitors of anti-apoptotic Bcl-2 proteins. J. Med. Chem. 49, 6139-6142.

Wiggins C.M., Tsvetkov P., Johnson M., Joyce C.L., Lamb C.A., Bryant N.J., Komander D., Shau Y., Cook S.J., 2011. BIM(EL), an intrinsically disordered protein, is degraded by 20S proteasomes in the absence of poly-ubiquitylation. J. Cell Sci. 124, 969-977.

Xu, J., Zhu, G. Y., Cao, D., Pan, H., & Li, Y.W., 2019. Gossypol overcomes EGFR-TKIs resistance in non-small cell lung cancer cells by targeting YAP/TAZ and EGFRL858R/T790M. Biomed. Pharmacother. 115, 108860.

Zhang, Z., Song, T., Zhang, T., Gao, J., Wu, G., An, L., Du, G., 2011. A novel BH3 mimetic S1 potently induces Bax/Bak-dependent apoptosis by targeting both Bcl-2 and Mcl-1. Int. J. Cancer 128, 1724-1735.

Zhang, Z., Song, T., Li, X., Wu, Z., Feng, Y., Xie, F., Chen, H., 2013. Novel soluble myeloid cell leukemia sequence 1 (Mcl-1) inhibitor (E, E)-2-(benzylaminocarbonyl)-3-styrylacrylonitrile (4g) developed using a fragment-based approach. Eur. J. Med. Chem. 59, 141-149.

Zhao L., Sun T., Pei J., Ouyang Q., 2015. Mutation-induced protein interaction kinetics changes affect apoptotic network dynamic properties and facilitate oncogenesis. Proc. Natl. Acad. Sci. USA 112, 4045-4054.
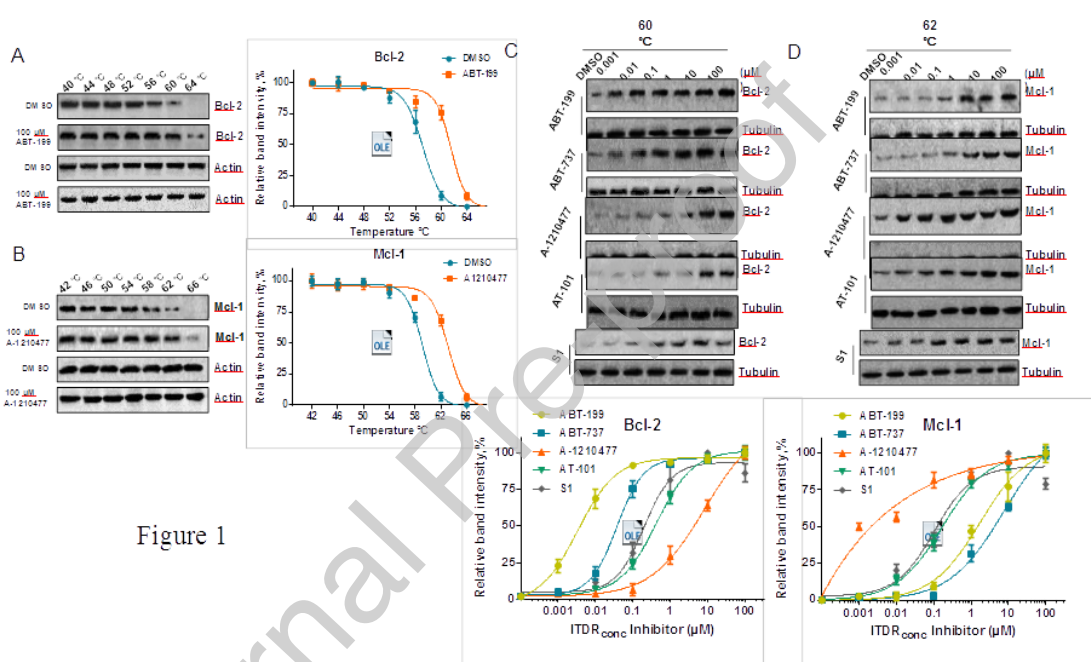
Figure Legends

Figure 1

Fig. 1. In-cell occupancy of Bcl-2 and Mcl-1 by small-molecule inhibitors as determined by CETSA assay. (A) MCF-7 cells were treated with DMSO, or 100 μM of ABT-199 for 1 h. Drug-treated cells were heated at gradient temperature from 40 °C to 64 °C for 3 min and then lysed, centrifuged to separate the soluble fractions from precipitates. The soluble fractions were analyzed by immunoblotting. Relative band intensities were plotted as a function of temperature followed a sigmoidal trend. The corresponding sigmoidal curve is on the right. (B) MCF-7 cells were treated with DMSO, or 100 μM of A-1210477 for 1 h. Drug-treated cells were heated at gradient temperature from 42 °C to 66 °C for 3 min and then lysed, centrifuged to separate the soluble fractions from precipitates. The soluble fractions were analyzed by immunoblotting. Relative band intensities were plotted as a function of temperature followed a sigmoidal trend. The corresponding sigmoidal curve is on the right. The corresponding sigmoidal curve is on the right. (C) MCF-7 cells were treated with small-molecule inhibitors (ABT-199, ABT-737, A-1210477, AT-101, **S1**) at the indicated doses (from 1nM to 100 μM) for 1 h and then heated at 60 °C. After cell lysis, the soluble fractions were collected for detecting Bcl-2 level by immunoblotting. Relative band intensities were plotted as a function of drug concentration followed a sigmoidal trend. The corresponding sigmoidal curve is on the right. (D) MCF-7 cells

14

were treated with small-molecule inhibitors (ABT-199, ABT-737, A-1210477, AT-101, **S1**) at the indicated doses (from 1nM to 100 μM) for 1 h and then heated at 62 °C,。 After cell lysis, the soluble fractions were collected for detecting Mcl-1 level by immunoblotting. Relative band intensities were plotted as a function of drug concentration followed a sigmoidal trend. The corresponding sigmoidal curve is on the right. All the same protein blots of different samples were exposed for the unified time. The CETSA data and ITDRF$_{CETSA}$ data were expressed as mean ± SD (n=3), the data (relative band intensities) from three independent assays were plotted using Graphpad Prism 6.0 software (GraphPad Software Inc., La Jolla, CA, USA) and fitted using a sigmoidal (variable slope) curve fit.
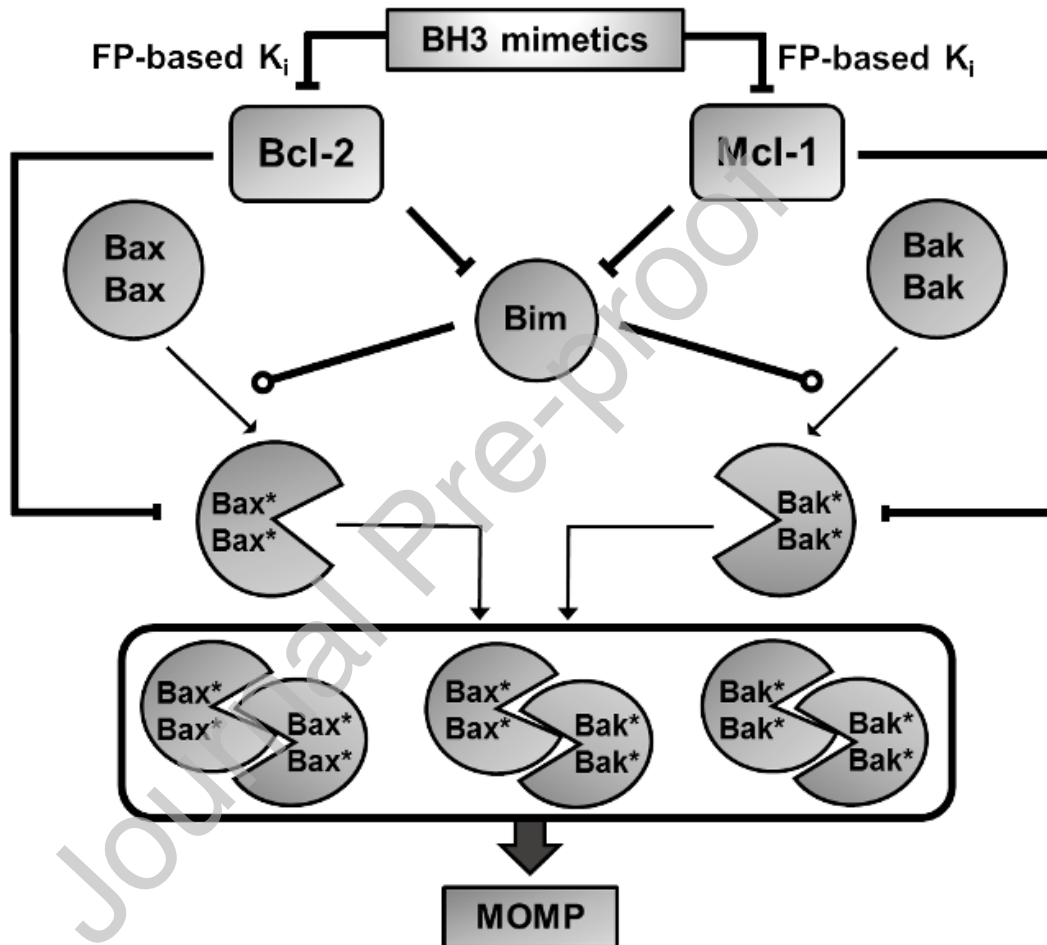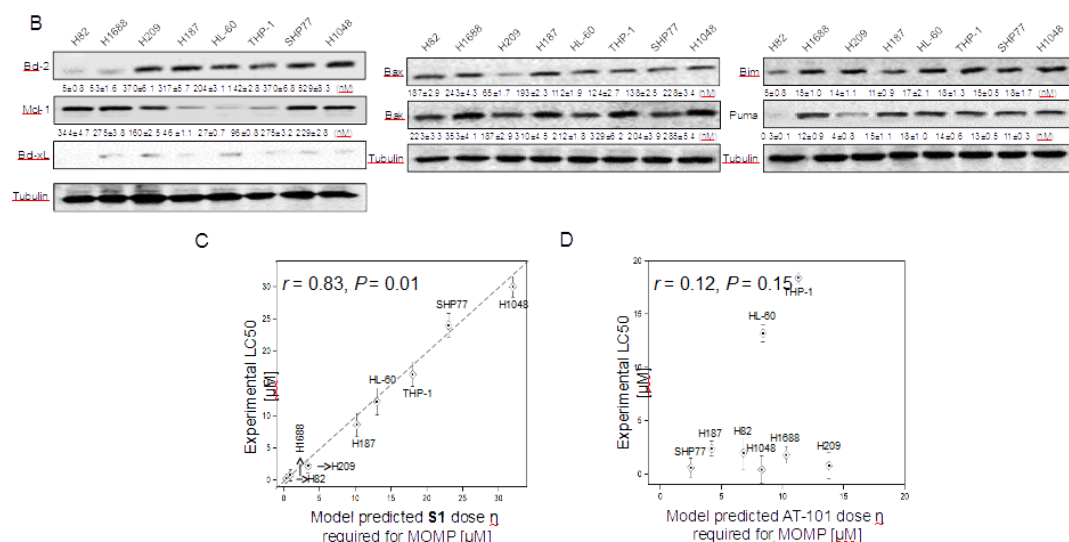

Figure 2

Figure 2

Fig. 2. S1, rather than AT-101 induced pharmacological response through an on-target mechanism. (A) Model of Bcl-2 protein interaction interfering by BH3 mimetics. (B) Quantitative immunoblotting analysis of the Bcl-2 family proteins (Bcl-2, Mcl-1, Bim, Puma, BAX and BAK) in the indicated 8 cell lines (H82, H1688, H209, H187, HL-60, THP-1, SHP77 and H1048). The intracellular protein concentrations were determined by comparison to signals from HL-60 cell extract and the numbers were listed underneath the blots. The results of protein concentrations are the mean ± SD (n=3). (C) The experimental LC_{50} values of 8 cells, assessed by cell apoptosis assay (48 h) of treatment with **S1**, was plotted against model predicted **S1** dose η required for MOMP. The results of experimental LC_{50} are the mean ± SD (n=3). Spearman's correlation (r) and P values are shown. (D) The experimental LC_{50} values of 8 cells, assessed by cell apoptosis assay (48 h) of treatment with AT-101, was plotted against model predicted AT-101 dose η required for MOMP. The results of experimental LC_{50} are the mean ± SD (n=3). Spearman's correlation (r) and P values are shown.
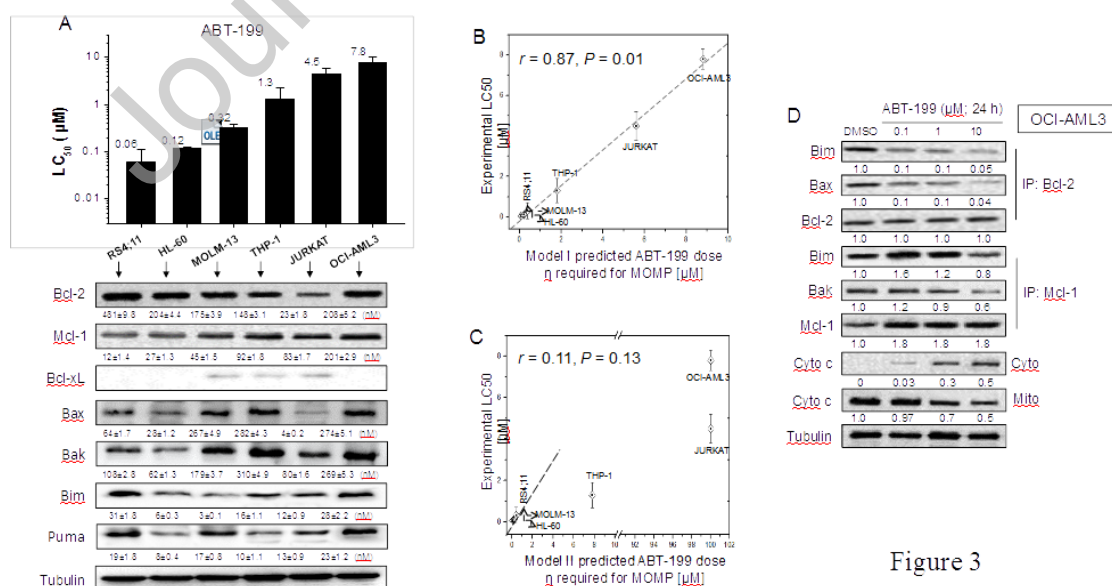

Figure 3

Fig. 3. ABT-199's lethality in leukemic subsets is achieved by dual engagement of Bcl-2 and

Mcl-1. (A) The experimental LC_{50} values of 6 various leukemic cell lines (RS4;11, HL-60, MOLM-13, THP-1, JURKAT, OCI-AML3) following treatment for 48 h with ABT-199 were determined by cell apoptosis assay. The numbers underneath the blots were intracellular protein concentrations of Bcl-2, Mcl-1, Bim, Puma, BAX and BAK in various cell lines. The results of experimental LC_{50} and protein concentrations are the mean $\pm$ SD (n=3). (B, C) The experimental LC_{50} value of 6 cells of treatment with ABT-199 was plotted against Model I (B) and Model II (C) predicted ABT-199 dose η required for MOMP. Spearman's correlation (r) and P values are shown. (D) OCI-AML3 cells were treated with ABT-199 for 24 h with indicated concentration. Bcl-2 and Mcl-1 immunoprecipitation assays were performed, and the immunoprecipitated fractions were analysed by immunoblotting for the indicated proteins. Cytochrome c release is assayed in parallel. The numbers underneath the blots were scanned and semi-quantified by densitometry, which were normalized to loading control (Tubulin).
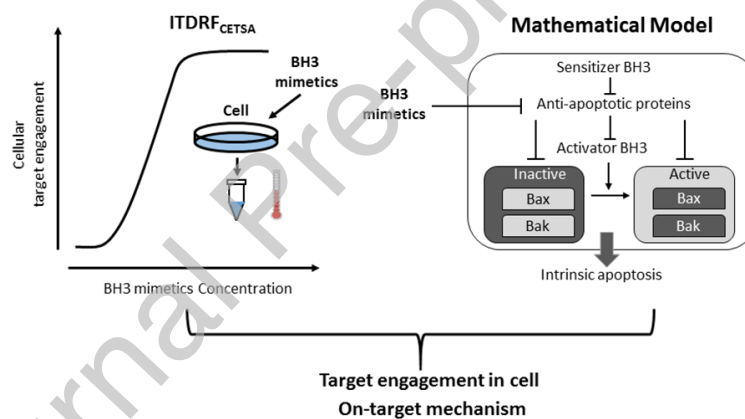
Graphical Abstract

Table 1 The binding affinities of BH3 mimetics to Mcl-1 and Bcl-2 in different assays

	Method	Mcl-1	Bcl-2
ABT-199	FP (K_i)	>780 nM (Lu., 2016)	1.20 nM (Casara., 2018)
	ITC (K_d)	ND	2.65 nM (Song., 2016)
	CETSA (IC_{50})	1.6 $\pm$ 0.9 μM	3.6 $\pm$ 1.1 nM
ABT-737	FP (K_i)	>10 μM (Milani., 2017)	34.9 nM (Park., 2013)
	ITC (K_d)	ND	21.3 nM (Song., 2016)
	CETSA (IC_{50})	8.3 $\pm$ 2.3 μM	40 $\pm$ 8 nM
A-1210477	FP (K_i)	28 nM (Kotschy., 2016)	>10 μM (Kotschy., 2016)
	MST (K_d)	740 nM (Milani., 2017)	ND
	SPR (K_d)	3.5 nM (Kotschy., 2016)	ND
	CETSA (IC_{50})	0.8 $\pm$ 0.1 nM	8.4 $\pm$ 6 μM
AT-101	FP (K_i)	180 nM (Wang., 2006)	320 nM (Wang., 2006)
	CETSA (IC_{50})	208 $\pm$ 47 nM	420 $\pm$ 85 nM

S1	FP (K_i)	58 nM (Zhang., 2011)	310 nM (Zhang., 2011)
	ITC (K_d)	960 nM (Zhang., 2013)	910 nM (Song., 2015)
	CETSA (IC_{50})	120 $\pm$ 29 nM	210 $\pm$ 67 nM

The K_i values were determined by FP and K_d values by direct binding ITC, MST, SPR. IC_{50} were calculated by $ITDRF_{CETSA}$. ND, not determined.